$FASn_{(1-x)}Ge_{(x)}I_3$ Hybrid Perovskite: Computational Insights into Wide-Bandgap Absorbers for Efficient Tandem Solar Cells

Hayat Arbouz*

Department of Physics, Faculty of Sciences, University of Blida1, Route de Soumaa B.P 270, 09000 Blida, Algeria

Abstract

The suitability of the lead-free hybrid perovskite $FASn_{1-x}Ge_xI_3$ as an efficient wide bandgap absorber for enhancing power conversion efficiency (PCE) in solar cells was examined, with the composition varied according to the germanium content x. To initiate the simulation study, a primary device architecture consisting of FTO/TiO_2/ $FASn_{1-x}Ge_xI_3$/Spiro-OMeTAD was established. Key photovoltaic parameters were systematically computed as functions of x to identify the optimal germanium concentration that maximizes PCE. The combined influence of the germanium ratio and absorber layer thickness on device performance was also investigated. In addition, multiple electron transport layer (ETL) and hole transport layer (HTL) materials, along with their thicknesses, were evaluated to design an improved device configuration exceeding the initial structure's performance. Under ideal conditions, the optimized structure achieved a power conversion efficiency of 33%, reflecting a 5% increase over the original design. However, when parasitic resistances were included to replicate realistic operational conditions, the PCE decreased to 24.44%. These findings demonstrate good agreement with results previously reported in the literature. This study aims to advance the development of stable, environmentally friendly wide bandgap perovskite solar cells that combine high efficiency with long-term sustainability.

Keywords: Hybrid Perovskite; Solar Cell; Simulation; Power Conversion; Photovoltaic

1. Introduction

Photovoltaic technology, which harnesses solar energy through semiconductor materials, has become integral to renewable energy development. Among emerging photovoltaic materials, perovskite solar cells (PSCs) have garnered significant attention [1]. These devices use perovskite-absorbers, characterized by their ABX_3 crystal lattice composition, which facilitate efficient light absorption and charge transport. Lead-halide perovskites such as methylammonium lead iodide ($MAPbI_3$) and formamidinium cesium lead iodide ($FA_{0.85}Cs_{0.15}PbI_3$) have demonstrated power conversion efficiencies (PCEs) exceeding 25%, showing improved stability under heat and humidity compared to $MAPbI_3$, maintaining about 85% of its performance after prolonged exposure [2]. Formamidinium (FA)-based perovskites have demonstrated significant improvements in both efficiency and stability compared to their methylammonium (MA) counterparts [3]. Incorporating FA cations into lead-halide perovskites enhances the crystalline grain size, which reduces moisture accumulation sites at grain boundaries and

mitigates rapid degradation under ambient conditions. Fabrication techniques for perovskite solar cells commonly include solution processing methods such as spin-coating and sequential deposition [4].

The tunability of perovskite bandgaps is a key feature enabling optimization for different photovoltaic applications [5]. This tunability has been exploited in tandem solar cells, where wide-bandgap perovskites (~1.77 eV) serve as top cells paired with lower-bandgap subcells, achieving efficiencies above 25% [6].

Despite the high efficiencies of lead-based perovskites, their toxicity and stability issues have driven research toward lead-free alternatives. Recent studies on environmentally friendly perovskite solar cells have mainly concentrated on substituting toxic lead (Pb) with safer elements such as tin (Sn), bismuth (Bi), antimony (Sb), and certain double perovskite formulations [7].

Tin-based perovskites have emerged as the most promising lead-free candidates, with reported efficiencies reaching approximately 15.3% for pure tin compositions $MASnI_3$ and up to 23.3% for $MAPbSnI_3$ tin-lead alloys, achieved through compositional engineering and defect passivation [8-9].

The majority of these non-toxic perovskite devices are fabricated via solution processing methods 10].

Formamidinium (FA)-based perovskites have demonstrated significant improvements in both efficiency and stability compared to their methylammonium (MA) counterparts. Incorporating FA cations into lead-halide perovskites enhances the crystalline grain size, which reduces moisture accumulation sites at grain boundaries and mitigates rapid degradation under ambient conditions [11].

Regarding lead-free FA-based perovskites, tin-based materials are the most promising alternatives, achieving up to approximately 15% [12]. The tunability of FA-based perovskites, combined with the ongoing development of lead-free formulations, offers a pathway to environmentally safer and stable photovoltaic devices without sacrificing too much performance.

This study undertakes the simulation of a single-junction solar cell featuring the hybrid perovskite absorber $FASn_{1-x}Ge_xI_3$, with its bandgap modulated by the germanium fraction represented by x-ratio.

Initially, the photovoltaic performance of the primary device, designed to begin the simulation study is calculated as a function of x to delineate the compositional range yielding optimal efficiency. Subsequently, the investigation expands to analyze the combined impact of absorber composition and thickness on key photovoltaic parameters, employing contour analysis to identify the parameter set that maximizes device performance. The third phase focuses on enhancing the device architecture by exploring alternative materials and thicknesses for the electron and hole transport layers (ETL and HTL), aiming to refine charge carrier extraction and improve overall efficiency. This process culminates in proposing an optimized structure that surpasses the baseline model. Finally, simulation results are benchmarked against previous experimental and theoretical studies to validate the approach. The objective is to provide comprehensive insight into how absorber composition influences solar cell performance while integrating material and architectural optimization strategies to achieve superior device efficiency.

2. Materials and Device Structure

2.1. $FASn_{1-x}Ge_xI_3$ Perovskite Material

In this work, we investigated the hybrid perovskite material $FASn_{1-x}Ge_xI_3$ as a promising absorber for single-junction solar cells. This material, with formamidinium as the organic cation, exhibits improved stability compared to its methylammonium-based counterpart. Importantly, lead is completely absent, replaced by a tunable mixture of tin and germanium. The proportion of these metals varies from the pure tin compound $FASnI_3$ to the pure germanium compound $FAGeI_3$, resulting in a band gap range from 1.4

eV to 2.2 eV depending on the germanium content. This composition is controlled by the x-ratio, which represents the germanium content relative to tin in the perovskite material, this later varies between 0 and 1. However, since this material is intended for use as a wide bandgap absorber in an upper part of a tandem solar cell, the variation in x was limited to a range between 0.3 and 0.7, which corresponds to a wide range of bandgap values between 1.6 eV and 1.8 eV, suitable for a top subcell of a tandem solar cell.

This work is a simulation. However, it is interesting to know how the $FASnGeI_3$ -based solar cell is made and what challenges are encountered during manufacture. Several works have suggested some manufacturing protocols for the successful deposition of $FaSnGeI_3$ films under inert conditions to minimize tin oxidation It was reported that the procedure is adapted from established methods for tin-based perovskites, modified to include germanium enabling the production of $FASnGeI_3$ films suitable for solar cells and other optoelectronic devices [13-15].

2.2. Structure and Device Simulation Parameters

Initially, a fundamental device architecture was developed, as illustrated in **Figure 1(a)**, which comprises the following sequential layers: FTO, TiO_2, $FASn_{1-x}Ge_xI_3$, Spiro-OMeTAD, and Au. The corresponding layer thicknesses are 350 nm, 100 nm, 500 nm, and 100 nm, respectively. The energy band alignment between the key layers of the device is presented in **Figure 1(b).**

Table 1 contains the physical parameters of the materials that make up the basic structure [16-18]. These are essential for calculating the cell's performance. **Table 2** shows the interfacial defects in the HTL absorber, and ETL absorber contacts. Figure 1(a) shows the energy band structure of the primary device FTO/TiO_2/ $FASn_{1-x}Ge_xI_3$/Spiro-OMeTAD/Au [19].

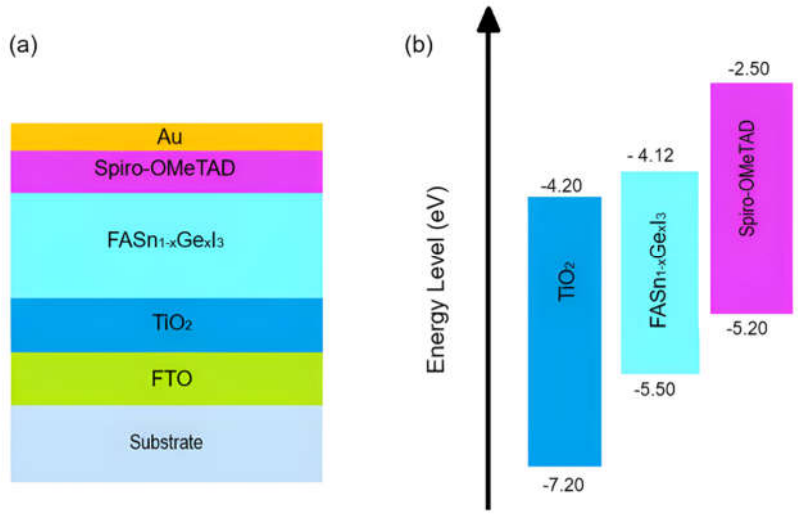

Figure 1. (a) Schematic Representation of the Primary Structure, **(b)** Energy Level Diagram

Table 1. Input Parameters for Materials used in the Primary Structure.

Input parameters	**FTO**	**TiO_2**	**$FASn_{1-x}Ge_xI_3$**	**Spiro-OMeTAD**
Thickness, d [nm]	350	100	800	300
Band gap, E_g [eV]	3.50	3.26	Variable	2.20
Electron Affinity, χ [eV]	4.00	4.00	Variable	2.90
Permittivity, ε_r	9	10	Variable	3.00
Electron mobility, μ_n [$cm^2\ V^{-1}s^{-1}$]	20	100	Variable	0.02
Hole mobility, μ_p [$cm^2\ V^{-1}s^{-1}$]	10	25	Variable	0.0002
CB Effective density of states, N_C [cm^{-3}]	2.2×10^{18}	2.0×10^{17}	3.0×10^{14}	1.0×10^{21}
VB Effective density of states, N_V [cm^{-3}]	1.8×10^{19}	10×10^{17}	1.0×10^{17}	1.0×10^{21}
Density of n-type doping, N_D [cm^{-3}]	1.0×10^{19}	1.0×10^{18}	/	/
Density of p-type doping, N_A [cm^{-3}]	/	/	1.0×10^{15}	1.0×10^{18}
Defect Density N_t [cm^{-3}]	/	1.0×10^{15}	1.0×10^{15}	1.0×10^{15}

Table 2 presents an overview of the interface parameters between the absorber layer and its adjoining ETL and HTL layers.

Table 2. Cell interface Parameters.

Parameters	**ETL**	**HTL**	**HTL/PL**	**PL/ETL**
Density of Defects, N_t [cm^{-3}]	10^{15}	10^{15}	10^{14}	10^{14}
Electron capture cross section, σ_n [cm^{-2}]	10^{-15}	10^{-15}	10^{-19}	10^{-19}
Hole capture cross section, σ_p [cm^{-2}]	10^{-15}	10^{-15}	10^{-18}	10^{-18}

3. Methodology

Numerical simulations of the studied perovskite solar cell (PSC) were conducted using Mathcad Prime 11, a software well-suited for rigorous mathematical modeling of photovoltaic devices [20]. This platform enables the development of comprehensive physical models. Furthermore, it supports parametric studies varying factors including active layer thickness, concentration of defects, doping levels, and band gap to optimize device performance.

Within this investigation, a robust model was constructed to predict the total photogenerated current densities of both electron and hole charge carriers, along with the device's current-voltage response and primary photovoltaic metrics. The foundation of the model lies in solving Poisson's equation coupled with continuity equations for charge carriers, alongside the drift-diffusion equations describing their transport dynamics [21]. Key parameters influencing the results include electron and hole mobilities μ_n and μ_p, diffusion coefficients D_n and D_p, carrier lifetimes, and diffusion lengths.

$$J_{ph} = q \int_{\lambda_{min}}^{\lambda_{max}} F(\lambda).EQE(\lambda)d\lambda \qquad (1)$$

λ_{min} and λ_{max} are minimum and maximum wavelengths,

J_{ph} is the total photogenerated current density, q is the electron charge, $F(\lambda)$ is the solar spectrum and $EQE(\lambda)$ is the external quantum efficiency of the cell [22].

$$R_{SRH} = \frac{n.p - n_i^2}{\tau_n.(n+n_i)+\tau_p.(p+p_i)} \qquad (2)$$

R_{SRH} is the recombination in the core of the absorber is due to a high density of defects.
n and p represent the concentrations of electrons and holes.
τ_n and τ_p are carrier life-times.

$$L_{n,p} = \sqrt{D_{n,p}.\tau_{n,p}} \quad (3)$$

The Tauc law was employed to calculate the absorption coefficient of the perovskite active layer and its adjacent layers [22].

$$\alpha(\lambda) = A.\left(\frac{hc}{\lambda} - E_g\right)^{1/2} \quad (4)$$

A: is a constant, and E_g is the energy of the bandgap.

$$J(V) = J_{ph} - J_0.\left(e^{\frac{q.(V-JR_s)}{2kT}} - 1\right) - \frac{V-J.R_s}{R_{sh}} \quad (5)$$

J(V) represent the equivalent circuit of the current-voltage characteristics where R_s and R_{sh} are parasitic resistances [23].

J_0 : is the recombination reverse dark current density.
The perovskite absorber studied in this work is tunable, based on its composition, specifically the ratio of germanium to tin. Consequently, changes in this compositional ratio directly influence its relevant physical parameters. The expressions below describe from **Equation 6** to **Equation 12**, the variation bandgap energy, electron affinity, density of acceptors, density of defects dielectric permittivity mobility of electrons and mobility of holes respectively, as functions of x-ratio.

$$E_g(x) = 1.4\,(1-x) + 2.2\,x - b.x.(1-x) \quad (6)$$
$$\chi(x) = 4.0\,(1-x) + 3.9\,x - b.x.(1-x) \quad (7)$$
$$N_a(x) = 10^{15}\,(1-x) + 10^{16}\,x \quad (8)$$
$$N_t(x) = 10^{14}\,(1-x) + 10^{16}\,x \quad (9)$$
$$\varepsilon_r(x) = 8.2\,(1-x) + 10\,x \quad (10)$$
$$\mu_n(x) = 22\,(1-x) + 16.2\,x \quad (11)$$
$$\mu_p(x) = 22\,(1-x) + 10.1\,x \quad (12)$$

The composition variation induces a change in the current-voltage J(V) characteristics and photovoltaic performance metrics.
This study's initial section examines how modifications in the active layer's composition influence the baseline device's efficiency, aiming to pinpoint the composition that maximizes performance.
The subsequent section explores key factors controlling the conversion efficiency.
The final section proposes an optimized device architecture derived from these insights, which demonstrates superior performance compared to the initial configuration with promising stability and lead-free environmental benefits.

4. Results and Discussions

4.1. Impact of the rate of Germanium in the Composition

The composition of the $FASn_{1-x}Ge_xI_3$ perovskite absorber is governed by the x-ratio, which varies between 0.3 and 0.7. This corresponds to a bandgap range of approximately 1.6 eV to 1.8 eV. **Figure 2** shows the current-voltage and power-voltage characteristics, respectively, for several values x.

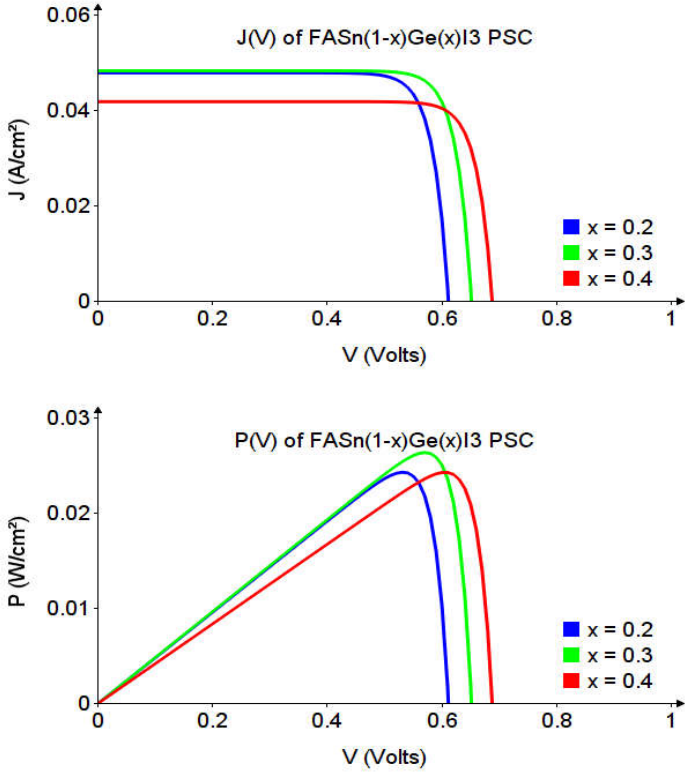

Figure 2. (a) Current-Voltage Curve, (b) Power-Voltage curve of $FASn_{1-x}Ge_xI_3$-based Solar Cell.

The curves illustrate the effect of composition changes on both characteristics. Notably, the maximum power point (P_{max}) increases as x rises from 0.2 to 0.3, but then declines when x moves from 0.3 to 0.4. This indicates that the optimal performance occurs for an x value between 0.3 and 0.4. Consequently, further investigation was carried out to accurately determine the concentration corresponding to the highest performance.

Optimizing the efficiency of solar cells based on the perovskite absorber $FASn_{1-x}Ge_xI_3$ requires careful adjustment of two fundamental parameters: the Ge content and the absorber thickness. The thickness is particularly important, as it must be sufficient to capture most of the incident solar spectrum, while avoiding excessive thickness that can lead to increased recombination and resistance losses [24].

This work investigates how thickness and composition together influence device performance, aiming to identify the optimal combination for achieving the highest efficiency. The analysis is conducted using contour plots to map these interdependent effects. To this end, the x ratio was varied from 0.3 to 0.7, while the thickness ranged from 0.5 to 2.5 µm. **Figure 3** illustrates the variations in photovoltaic parameters resulting from the combined effects of these two factors.

Contour plotting provides a clear visualization of regions corresponding to optimal device performance. The analysis indicates that changes in composition have a more substantial impact than variations in thickness. Photovoltaic parameters tend to reach stability at a thickness of approximately 1.5 µm. At this point, the short-circuit current density and power conversion efficiency peak at lower composition values

($x \leq 0.4$) and subsequently decrease. In contrast, the highest short-circuit voltage and fill factor values are observed within the composition range of 0.6 to 0.7. Numerical evaluation of the data identifies the composition ratio x = 0.35 as the condition under which maximum conversion efficiency is achieved.

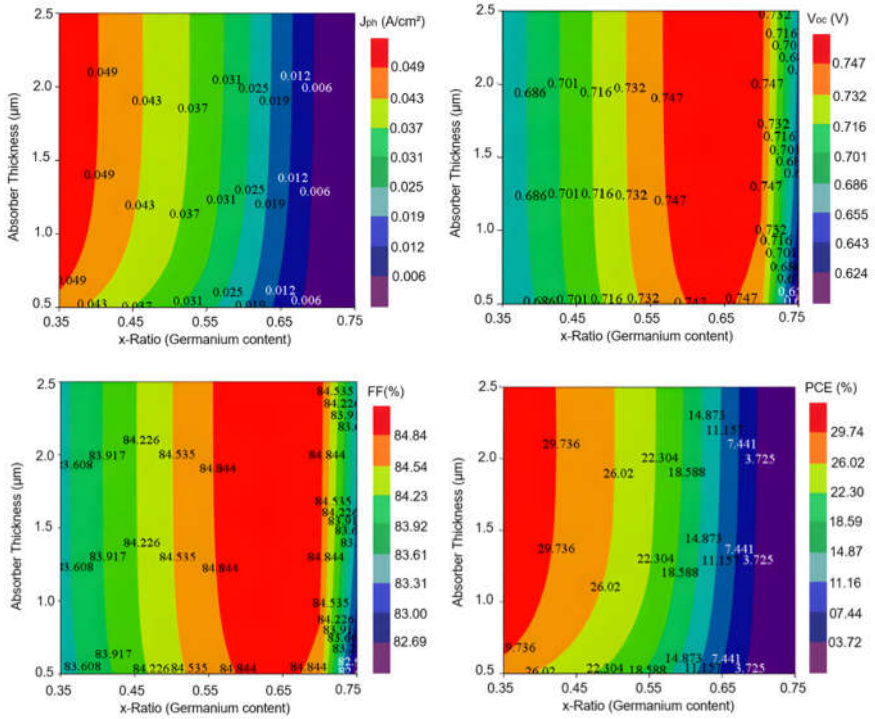

Figure 3. Contour Plot Analysis of PCE as a function of the Absorber Thickness and x-ratio.

This analysis not only evaluates performance based on the ability to adjust the band gap according to variations in composition in order to identify the optimal germanium content for maximum efficiency, but also assesses the behavior of photovoltaic parameters according to germanium content. This makes it possible to define precise compositions for the upper and lower subcells in a tandem solar cell structure.

4.2. Simultaneous impact of ETL and Absorber Thicknesses on PCE

The efficiency of perovskite solar cells is affected by multiple factors, including the alignment of energy bands, the mobility of electrons, and the band gap of materials used in the electron transport layer (ETL). Therefore, optimizing the ETL is critical to achieving effective electron transport properties and optimal device performance. Titanium dioxide (TiO_2), commonly applied as an ETL in standard configurations, demonstrates but tends to suffer from instability and mechanical rigidity due to its requirement for high-temperature annealing [24]. This has prompted ongoing efforts to identify ETL materials that deliver a desirable combination of efficiency, longevity, and robustness.

Inorganic metal oxides such as zinc oxide (ZnO) and tin oxide (SnO_2) [24] are preferred for their high electron mobility, which contributes to enhancing overall cell efficiency. Emerging alternatives like lanthanum-doped barium stannate (La:$BaSnO_3$ or LBSO) show promise due to their superior electron mobility and lower photocatalytic activity [25]. On the other hand, PC60BM is gradually losing favor

because of its expense and sensitivity issues [26].

Other zinc-based ETLs such as ZnMgO, and ZnSe combine good electronic properties and tunable energy levels [27]. Cadmium-based electron transport layers (ETLs) like CdS, CdZnS, and CdTe offer promising options for developing scalable, efficient, and affordable perovskite solar cells [28].

Indium-based electron transport layers (ETLs) such as In_2S_3 and IGZO are a good alternative to traditional materials used in ETLs due to their excellent electrical conductivity and high optical transparency [29]. It has also been reported that tin-based ETLs such as SnO_2 and SnS_2 are excellent choices promising candidates in development for efficient and stable electron transport layers with good processing versatility.

Finally, among the tungsten-based materials, Tungsten trioxide (WO_3) and tungsten disulfide (WS_2) are two distinct tungsten-based materials used in electron transport layers (ETLs) for solar cells [30].

The materials mentioned above were studied as ETLs in our study with the aim of replacing the TiO_2 used in the base structure. The approach consists of finding the materials best suited to the $FASn_{0.65}Ge_{0.35}I_3$ absorber. To do this, two important factors must be taken into consideration. The thickness of the two materials that make up the hetero-junction and ensure the generation, extraction, and transport of electrons, and the correct alignment of the energy bands at the ETL/absorber interface, which promotes the passage of electrons and the blocking of holes.

To this end, a contour analysis representing the conversion efficiency as a function of the thicknesses involved was used to more clearly visualize the thickness ranges that give the best results. Finding are represented in **Figure 3**. The curves obtained provide us with information on various points. The most visible is the area between the different thickness ranges where the highest efficiency is achieved. In fact, we observe that maximum efficiency is achieved for all materials when the absorber thickness is approximately 1 µm. However, some materials appear to be little or not at all sensitive to increases in the thickness of the ETL layer. These are SnO_2, LBSO, ZnO, ZnMgO, and ZnSe, respectively.

However, the conversion efficiency of structures whose ETL layer consists of In_2S_3, WS_2, CdTe, SnS_2, WO_3, and the polymers PC60BM and C60 tend to deteriorate as the thickness of the latter increases. Consequently, optimizing the thicknesses of the absorber and ETL is essential to maintain the highest conversion efficiency. That said, it is simpler to keep the ETL layer as thin as possible within the limits allowed by the manufacturing process, which is 50 nm in this case. According to the results, the best efficiency was recorded with CdZnS as the ETL, taking an optimal absorber thickness at which the efficiency stabilizes, i.e., at 1.15 µm for a CdZnS thickness of 50 nm, an efficiency value of 33% is obtained and a favorable alignment of 0.4 eV of the conduction bands at the ETL/absorber interface.

4.3. Optimization of the HTL's Materiel

The hole transport layer (HTL) is essential in perovskite solar cells (PSCs) as it facilitates the efficient extraction and transport of holes from the perovskite absorber to the electrode, thus enabling effective charge separation and minimizing recombination losses [31]. Optimizing the HTL is crucial because it directly influences the photovoltaic performance. Additionally, the HTL serves as a protective barrier that enhances the chemical stability of the perovskite layer by preventing degradation induced by moisture or other environmental factors. The choice of HTL material must ensure appropriate energy level alignment with the perovskite's valence band to promote favorable charge transfer while maintaining high hole mobility and structural integrity. Therefore, tailoring the HTL characteristics is a key strategy for advancing stable and high-performance PSC devices.

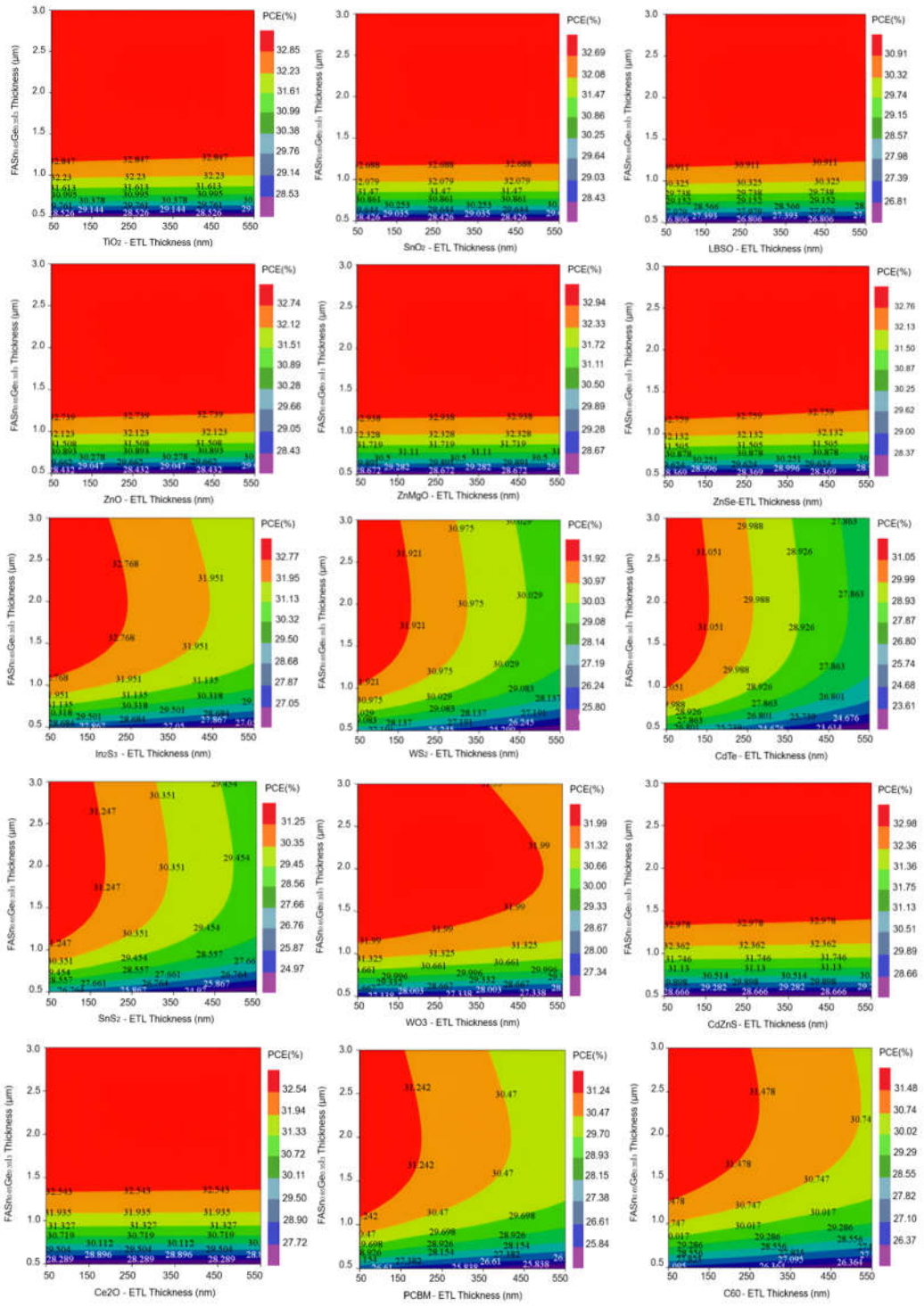

Figure 3. Contour Plot Analysis of PCE as a function of Absorber and ETL Thicknesses.

Spiro-OMeTAD, used in the primary device of this work, remains a leading HTL material due to its efficient hole transport and processing characteristics, but its stability and cost challenges motivate ongoing research into alternative materials and doping methods for perovskite solar cells [32].

In this part of the work, several potential organic and inorganic materials, detailed below, were studied as HTL. Organic HTL materials such as PEDOT:PSS and P3HT are widely used in solar cells [33-34].

Copper-based HTLs are very promising materials. Copper(I) oxide (Cu_2O) and copper thiocyanate (CuSCN) are abundant and non-toxic p-type materials characterized by wide bandgaps, high acceptor densities, and superior charge carrier mobility [35]. CuSCN typically demonstrates enhanced stability and improved photovoltaic performance relative to Cu_2O, contributing to higher power conversion efficiencies in optimized perovskite solar cells (PSCs). Both materials benefit from low-cost synthesis routes and compatibility with low-temperature processing techniques.

Copper (II) oxide (CuO) exhibits a wide bandgap and notable thermal stability, attributes that have been exploited to improve both the photovoltaic efficiency and thermal resilience of PSC devices. Copper iodide (CuI) possesses high electrical conductivity, excellent optical transparency, and rapid hole mobility, rendering it well suited for application as a hole transport layer (HTL) [35].

Furthermore, CuI can be processed at relatively low temperatures and offers superior environmental stability and simpler fabrication compared to commonly used organic HTLs such as PEDOT:PSS. Recently, copper antimony sulfide ($CuSbS_2$) has emerged as a promising HTL material due to its favorable optical absorption and electronic properties, which are compatible with PSC architectures [36].

Vanadium pentoxide (V_2O_5) is also widely recognized as an effective hole transport layer (HTL) material across various solar cell technologies. The incorporation of V_2O_5 HTLs exhibit superior resistance to moisture and thermal degradation compared to those utilizing conventional organic HTLs, while simultaneously improving key photovoltaic parameters and overall power conversion efficiency (PCE). And finally, Compared to commonly used organic HTLs, NiO_x offers superior thermal and environmental stability, reducing device degradation due to moisture and heat [37].

The performance of solar cell structures comprising the above-mentioned HTL materials is shown in the **Table 3.** It should be noted that, during the performance calculations, the 100 nm thick TiO_2 layer was retained in the structure and the thickness of the $FASn_{0.65}$ $Ge_{0.35}I_3$ absorber was maintained at 500 nm.

The results showed comparable performance across all organic and inorganic hole transport layer (HTL) materials, each demonstrating favorable valence band alignment. Notably, the highest conversion efficiency was recorded with $CuSbS_2$ at 28.12%, closely followed by Cu_2O with an efficiency of 28.11%.

The thickness of the HTL layer must also be optimized for optimal hole transport. The current-voltage and power voltage characteristics of the structure comprising the HTL Cu_2SbS_2 material were calculated at different thicknesses.

The results are shown in **Figure 4.** The latter reveals an increase in photocurrent density as the thickness of the HTL layer increases, which can be explained by improved hole transport that adds to the total photocurrent of the cell. However, it can be seen that saturation begins to occur above a thickness of 350 nm. The same behavior is observed with regard to maximum operating power. However, the open-circuit voltage does not appear to change with increasing thickness. Based on these observations, it would be advisable to increase the thickness of the HTL layer to 350 nm in order to achieve better performance.

Table 3. Performance of Structures based on alternative HTLs

HTL Material	**J_{ph} (mA/cm²)**	**V_{oc} (V)**	**FF (%)**	**PCE (%)**	**ΔE_v (eV)**
Spiro-OMeTAD	46.99	0.671	83.4	28.04	0.180
Pedot:PSS	46.99	0.671	83.4	28.04	0.170
P3HT	46.96	0.671	83.4	28.02	0.071

Cu_2O	47.10	0.671	83.4	28.11	0.571
CuO	47.06	0.671	83.4	28.09	0.450
CuI	46.99	0.671	83.4	28.04	0.170
$CuSbS_2$	47.12	0.671	83.4	28.12	0.351
CuSCN	46.99	0.671	83.4	28.04	0.170
V_2O_5	47.06	0.671	83.4	28.09	-0.430
NiO	47.01	0.671	83.4	28.06	0.271

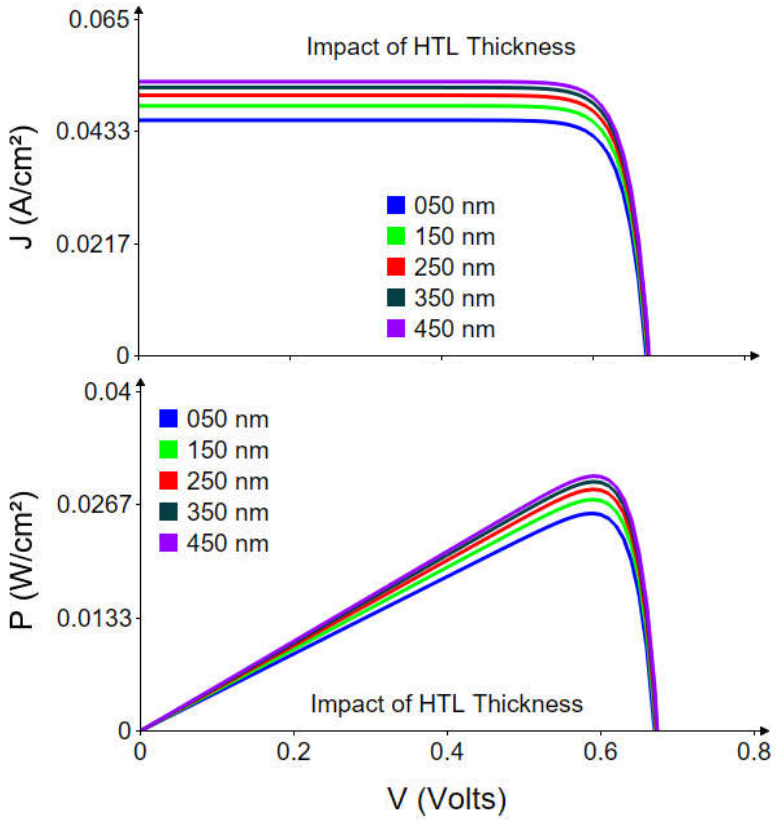

Figure 4. The Impact of HTL's Thickness on Current –Voltage and Power-Voltage Characteristics of the stucture.

The latter reveals an increase in photocurrent density as the thickness of the HTL layer increases, which can be explained by improved hole transport that adds to the total photocurrent of the cell. However, it can be seen that saturation begins to occur above a thickness of 350 nm. The same behavior is observed with regard to maximum operating power. However, the open-circuit voltage does not appear to change with increasing thickness. Based on these observations, it would be advisable to increase the thickness of the HTL layer to 350 nm in order to achieve better performance.

5. Optimization and Comparative Analysis

Simulation findings helped to design an optimized device employing a $FASn_{1-x}Ge_xI_3$ perovskite absorber layer with a thickness of 1.15 µm, and x = 0.35, interfaced with a 50 nm CdZnS electron transport layer (ETL) and a 350 nm $CuSbS_2$ hole transport layer (HTL). A high power conversion efficiency of 33.44% was achieved in ideal conditions, alongside the key photovoltaic indicators detailed in **Table 4.**

For a rigorous comparison with existing studies on related device architectures, incorporation of parasitic resistance effects is necessary [38]. Series resistance (R_s) originates from resistive losses in the conductive layers, interfaces, and contact regions within the cell. In contrast, shunt resistance (R_{sh}) reflects defect-induced leakage pathways; low R_{sh} values cause reductions in the open-circuit voltage (V_{OC}) and Fill Factor.

The results shown in **Table 4** show a decrease in photovoltaic parameters when parasitic resistances are taken into account; the conversion efficiency decreases to 24%.

Figure 5 compares the current-voltage characteristics of the optimized device under ideal conditions against those obtained when accounting for parasitic resistances, using R_s = 3 Ω and R_{sh} = 800 Ω.

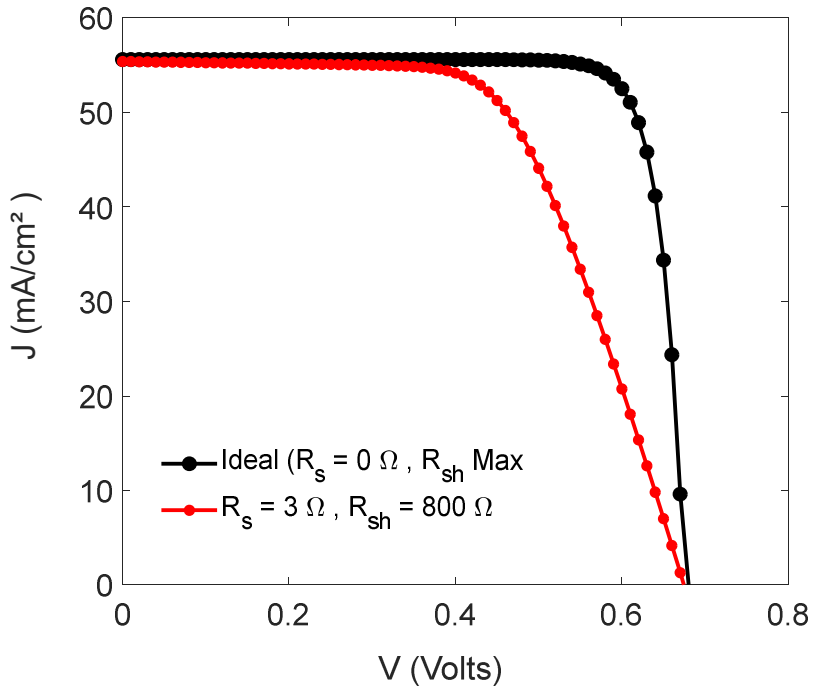

Figure 5. Comparison of J-V Characteristics of Optimized Solar Cell Devices Under Ideal and Real Conditions.

Table 4. Comparison of Key Photovoltaic Parameter Results.

Cell's Structure	**J_{ph} (mA/cm²)**	**V_{oc} (V)**	**FF (%)**	**PCE (%)**
Primary (This Work)	46.99	0.671	83.4	28.04
Optimized (This Work – Ideal)	55.61	0.675	83.5	33.44
Optimized (This Work – Real)	54.55	0.671	62.3	24.34
[39]	29.40	1.04	82.24	24.45

[40]	30.79	1.143	84.56	24.54
[41]	30.67	0.938	87.1	24.87

Table. 4 presents the key findings of this study. Under ideal conditions, and at room temperature, the primary solar cell structure achieved an efficiency of 28%. However, through simulation and optimization, an enhanced structure was developed that outperforms the original by over 5%, reaching a conversion efficiency exceeding 33%. In contrast, under real operating conditions where parasitic resistances are considered, the maximum attainable efficiency decreases to 24.44%.

Comparison with related studies on similar perovskite solar cells reveals a consistent correlation in performance metrics, particularly regarding power conversion efficiency. This investigation underscores the potential of this device architecture for the advancement of high-efficiency solar cells employing cost-effective and environmentally benign materials. Moreover, owing to its wide bandgap, the studied configuration is suitable as the top subcell in tandem solar cell configurations.

6. Conclusion

In this study, the lead-free hybrid perovskite material $FASn_{1-x}Ge_xI_3$ was investigated as a promising wide bandgap absorber for high-efficiency solar cell devices. This material exhibits enhanced stability compared to its methylammonium-based counterparts and presents tunable physical properties that depend on the germanium content, denoted by the compositional parameter x. Photovoltaic performance metrics of the primary device configuration, $FTO/TiO_2/FASn_{1-x}Ge_xI_3$/Spiro-OMeTAD, were systematically evaluated as a function of x, with an optimal composition at x = 0.35 yielding a maximum power conversion efficiency (PCE) of 28%. Further analysis involved exploring various electron transport layer (ETL) and hole transport layer (HTL) materials along with their corresponding thicknesses, leading to the design of an optimized device structure incorporating an $FTO/CdZnS/ FASn_{0.65}Ge_{0.35}I_3/CuSbS_2$. This enhanced configuration demonstrated improved performance, achieving an ideal PCE of 33%. However, when parasitic resistances were accounted for to simulate realistic operating conditions, the efficiency decreased to 24%. The results obtained exhibit strong agreement with previously published data. This work contributes to the development of stable, eco-friendly wide bandgap perovskite solar cells, aiming to merge high photovoltaic efficiency with sustainability.

Funding: There is no funding for this paper.

Authors' contributions: Hayat Arbouz: Conceptualization, Methodology, Software, Investigation, Writing, Reviewing and Editing.

Conflicts of Interest: The author declares no conflict of interest

Ethical approval: The conducted research is not related to either human or animal use

Data Availability: Derived data supporting the findings of this study are available from the corresponding author on request.

References

[1] Panneerselvam Priya, & Stonier, A. A. (2025). Emerging innovations in solar photovoltaic (PV) technologies: The perovskite solar cells and more. Energy Reports, 14, 216-242. https://doi.org/10.1016/j.egyr.2025.06.003

[2] Qiu, Z., Li, N., Huang, Z., Chen, Q., & Zhou, H. (2020). Recent advances in improving phase stability of perovskite solar cells. Small Methods, 4. https://doi.org/10.1002/smtd.201900877

[3] Mehra, S., Mamta, V. N. Singh, Gupta, G., Srivastava, A. K., & Sharma, S. N. (2023). Experimental analysis of methylammonium and formamidinium-based halide perovskite properties for optoelectronic applications. Heliyon, 9(11), e21701. https://doi.org/10.1016/j.heliyon.2023.e21701

[4] Arbouz, H. (2023). Optimization of lead-free CsSnI3-based perovskite solar cell structure. Applied Rheology, 33(1), 20220138. https://doi.org/10.1515/arh-2022-0138

[5] Raju, T. D., Murugadoss, V., Nirmal, K. A., Dongale, T. D., Kesavan, A. V., & Kim, T. G. (2025). Advancements in perovskites for solar cell commercialization: A review. Advanced Powder Materials, 4(2), 100275. https://doi.org/10.1016/j.apmate.2025.100275

[6] Li, Q., Chai, W., Luo, X., Zhu, W., Chen, D., Zhou, L., Xi, H., Dong, H., Zhang, C., & Hao, Y. (2025). Wide-bandgap subcells for all-perovskite tandem solar cells: Recent advances, challenges, and future perspectives. Energies, 18(10), 2415. https://doi.org/10.3390/en18102415

[7] Abdelghafar, A. A., Mdallal, A., Allam, M. A., Al Ali, H., Alami, A. H., Abdelkareem, M. A., & Olabi, A. G. (2025). Passivation strategies in lead-free perovskite solar cells: Towards efficient and stable photovoltaic devices. Energy Nexus, 19, 100487. https://doi.org/10.1016/j.nexus.2025.100487

[8] Ke, W., Stoumpos, C., Spanopoulos, I., Mao, L., Chen, M., Wasielewski, M., & Kanatzidis, M. (2017). Efficient lead-free solar cells based on hollow {en}MASnI3 perovskites. Journal of the American Chemical Society, 139. https://doi.org/10.1021/jacs.7b09018

[9] Zhang, T., Wang, F., Chen, H., Qian, F., Li, J., Zheng, H., Yuan, S., Peng, X., Wang, Y., Huang, J., Cui, H., Yu, Z., Chen, Z. D., & Li, S. (2023). Synchronized B-site alloying for high-efficiency inorganic tin–lead perovskite solar cells. Applied Physics Reviews, 10(4), 041417. https://doi.org/10.1063/5.0162009

[10] Ji, R., Mallick, A., Rivkin, B., Yuce-Cakir, H., Jurchescu, O. D., & Vaynzof, Y. (2025). Solvent-free fabrication methods of metal halide perovskites. Advanced Materials. Advance online publication. https://doi.org/10.1002/adma.202416604

[11] Raju, T. D., Murugadoss, V., Nirmal, K. A., Dongale, T. D., Kesavan, A. V., & Kim, T. G. (2025). Advancements in perovskites for solar cell commercialization: A review. Advanced Powder Materials, 4(2), 100275. https://doi.org/10.1016/j.apmate.2025.100275

[12] Kavitha, M. V., & Sebastian, K. S. (2025). Device modelling and performance enhancement of FASnI3-based perovskite solar cell with diverse, compatible charge transport layers. Results in Optics, 18, 100783. https://doi.org/10.1016/j.rio.2025.100783

[13] Haque, M. M., Amanullah, M., Mia, M. R., & Islam, M. R. (2024). Strain effect on the electronic and optical characteristics of FAGeX3 (X=Cl, Br, and I) perovskite materials: DFT analysis. Heliyon, 10(21), e39799. https://doi.org/10.1016/j.heliyon.2024.e39799

[14] Lee, J.-W., & Park, N.-G. (2015). Two-step deposition method for high-efficiency perovskite solar cells. MRS Bulletin, 40(8), 654–659. https://doi.org/10.1557/mrs.2015.166

[15] Gantumur, M., Shahiduzzaman, M., Hossain, M. I., Akhtaruzzaman, M., Nakano, M., Karakawa, M., Nunzi, J. M., & Taima, T. (2025). Revolutionizing light capture: A comprehensive review of back-contact perovskite solar cell architectures. Materials Today. https://doi.org/10.1016/j.mattod.2025.08.017

[16] Helander, M., Greiner, M., Wang, Z. B., Tang, W., & Lu, Z. H. (2011). Work function of fluorine doped tin oxide. Journal of Vacuum Science & Technology A: Vacuum, Surfaces, and Films, 29, 011019. https://doi.org/10.1116/1.3525641

[17] Rehman, U. U., Almousa, N., Sahar, K. U., Ashfaq, A., Mahmood, K., Shokralla, E. A., Al-Buriahi, M. S., Alrowaili, Z. A., Capangpangan, R. Y., & Alguno, A. C. (2023). Optimizing the efficiency of lead-free Cs2TiI6-based double halide perovskite solar cells using SCAPS-1D. Energy Technology, 11, 2300459. https://doi.org/10.1002/ente.202300459

[18] Moiz, S. A., Alahmadi, A. N. M., & Aljohani, A. J. (2021). Design of a novel lead-free perovskite solar cell for 17.83% efficiency. IEEE Access, 9, 54254–54263. https://doi.org/10.1109/access.2021.3070112

[19] Shimul, A. I., Ghosh, A., Bappy, M. A., Islam, M. B., Aljazzar, S., Al-Humaid, J., & Mukhrish, Y. (2025). Numerical insights into CsSnBr3 perovskite solar cells: Evaluating organic charge transport layers using DFT, SCAPS-1D, and wxAMPS simulations. Optics Communications, 579, 131558. https://doi.org/10.1016/j.optcom.2025.131558

[20] Mathcad. (n.d.). Retrieved from https://www.mathcad.com/

[21] Richardson, G., & Walker, A. (2016). Drift diffusion modelling of charge transport in photovoltaic devices. In Unconventional Thin Film Photovoltaics (pp. 297–331). Royal Society of Chemistry. https://doi.org/10.1039/9781782624066-00297

[22] Arbouz H. Optimization study of lead-free Cssngei3 perovskite based solar cell structures. Int J Adv Sci Eng Technol. 2024;12(2):127-34

[23] Meyer, E. L., Jakalase, S., Nqombolo, A., Rono, N., & Agoro, M. A. (2025). The numerical simulation of a non-fullerene thin-film organic solar cell with Cu2FeSnS4 (CFTS) kesterite as a hole transport layer using SCAPS-1D. Coatings, 15(3), 266. https://doi.org/10.3390/coatings15030266

[24] Qiu, C., Wu, Y., Song, J., Wang, W., & Li, Z. (2022). Efficient planar perovskite solar cells with ZnO electron transport layer. Coatings, 12(12), 1981. https://doi.org/10.3390/coatings12121981

[25] Hossain, M., Sadat, K., Uddin, M., et al. (2025). An investigation of hole transport layers and electron transport layers to produce highly efficient K2TiI6-based perovskite solar cells. Scientific Reports, 15, 19014. https://doi.org/10.1038/s41598-025-98351-y

[26] Richards, J., Rice, A., Nelson, R., Kim, F., Jenekhe, S., Luscombe, C., & Pozzo, L. (2013). Modification of PCBM crystallization via incorporation of C60 in polymer/fullerene solar cells. Advanced Functional Materials, 23. https://doi.org/10.1002/adfm.201201100

[27] Zhang, Q., Gu, X., Zhang, Q., Jiang, J., Jin, X., Li, F., Chen, Z., Zhao, F., & Li, Q. (2018). ZnMgO:ZnO composite films for fast electron transport and high charge balance in quantum dot light emitting diodes. Optical Materials Express, 8, 909-918. https://doi.org/10.1364/OME.8.000909

[28] Xu, X.-B., Wang, X.-Y., Gu, W.-P., Quan, S., & Zhang, Z. (2017). Study on influences of CdZnS buffer layer on CdTe solar cells. Superlattices and Microstructures, 109, 463-469. https://doi.org/10.1016/j.spmi.2017.05.033

[29] Elhadi, M., Tazwar, M. T., Zishan, A. S., Faruque, M. A., Anonto, H. Z., Eid, M. M. A., Rashed, A. N. Z., Rahman, M. F., & Harun-Or-Rashid, M. (2025). Optimization and comparative analysis of electron transport layers for high-performance InGeCl3-based perovskite solar cells. ChemistrySelect, 10, e01364. https://doi.org/10.1002/slct.202501364

[30] Abbas, K., & Bahrami, A. (n.d.). Investigating the potential of WO3 and WS2 as Cd-free buffer layers in Sb2Se3-based thin-film solar cells: A numerical study with SCAPS-1D software. SSRN. https://doi.org/10.2139/ssrn.4700811

[31] Srivastava, A., Kasliwal, M., & Shirage, P. M. (2025). From HTL to HTL-free: Experimental and numerically modelled performance dynamics of Cs2AgBiBr6 double perovskite solar cells. Solar Energy, 298, 113733. https://doi.org/10.1016/j.solener.2025.113733

[32] Nakka, L., Cheng, Y., Aberle, A., & Lin, F. (2022). Analytical review of Spiro-OMeTAD hole transport materials: Paths toward stable and efficient perovskite solar cells. Advanced Energy and Sustainability Research, 3, 2200045. https://doi.org/10.1002/aesr.202200045

[33] Reza, K., Mabrouk, S., & Qiao, Q. (2018). A review on tailoring PEDOT:PSS layer for improved performance of perovskite solar cells. Proceedings of the Nature Research Society, 2, 02004. https://doi.org/10.11605/j.pnrs.201802004

[34] Singh, N., Dubey, K. C., Singh, S. K., Srivastava, A., Wadhwani, N., & Shukla, R. K. (2025). Optimizing parameters for enhanced conversion efficiency in P3HT/PCBM-based solar cells through computer simulations. Next Research, 2(3), 100601. https://doi.org/10.1016/j.nexres.2025.100601

[35] Mbese, J. Z. (2025). Advancements in inorganic hole-transport materials for perovskite solar cells: A comparative review. Energies, 18(9), 2374. https://doi.org/10.3390/en18092374

[36] Shivesh, K., Alam, I., Kushwaha, A. K., Kumar, M., & Singh, S. V. (2022). Investigating the theoretical performance of Cs2TiBr6-based perovskite solar cell with La-doped BaSnO3 and CuSbS2 as the charge transport layers. International Journal of Energy Research, 46(5), 6045-6064. https://doi.org/10.1002/er.7546

[37] Cai, X., Hu, T., Hou, H., Zhu, P., Liu, R., Peng, J., Luo, W., & Yu, H. (2023). A review for nickel oxide hole transport layer and its application in halide perovskite solar cells. Materials Today Sustainability, 23, 100438. https://doi.org/10.1016/j.mtsust.2023.100438

[38] Chauhan, A., Oudhia, A., Shrivastav, A. K., & Tirkey, O. S. (2023). Performance enhancement of an all-inorganic perovskite solar cell by using SCAPS and DFT extracted parameters of CuX (X = I, Cl, Br). Materials Chemistry and Physics, 309, 128327. https://doi.org/10.1016/j.matchemphys.2023.128327

[39] Ke, W., et al. (2017). Efficient lead-free solar cells based on Hollow {en}MASnI3 perovskites. Journal of the American Chemical Society, 139, 14800–14806.

[40] Singh, A. K., Srivastava, S., Mahapatra, A., Baral, J. K., & Pradhan, B. (2021). Performance optimization of lead free-MASnI3 based solar cell with 27% efficiency by numerical simulation. Optical Materials, 117, 111193.

[41] Tara, A., Bharti, V., Sharma, S., & Gupta, R. (2021). Device simulation of FASnI3 based perovskite solar cell with Zn(O0.3, S0.7) as electron transport layer using SCAPS-1D. Optical Materials, 119, 11136